# Breaking of Coulomb blockade by macrospin-assisted tunneling

Tim Ludwig[1] and Rembert A. Duine[1,2]
[1]*Institute for Theoretical Physics, Utrecht University, Princetonplein 5, 3584 CC Utrecht, Netherlands*
[2]*Department of Applied Physics, Eindhoven University of Technology, P.O. Box 513, 5600 MB Eindhoven, Netherlands*

(Received 9 December 2020; accepted 28 April 2021; published 2 June 2021)

A magnet with precessing magnetization pumps a spin current into adjacent leads. As a special case of this spin pumping, a precessing macrospin (magnetization) can assist electrons in tunneling. In small systems, however, the Coulomb blockade effect can block the transport of electrons. Here, we investigate the competition between macrospin-assisted tunneling and the Coulomb blockade for the simplest system where both effects meet; namely, for a single tunnel junction between a normal metal and a metallic ferromagnet with precessing magnetization. By combining Fermi's golden rule with magnetization dynamics and charging effects, we show that the macrospin-assisted tunneling can soften or even break the Coulomb blockade. The details of these effects—softening and breaking of the Coulomb blockade—depend on the macrospin dynamics. This allows us, for example, to measure the macrospin dynamics via a system's current-voltage characteristics. It also allows us to control a spin current electrically. From a general perspective, our results provide a platform for the interplay between spintronics and electronics on the mesoscopic scale. We expect our work to provide a basis for the study of Coulomb blockade in more complicated spintronic systems.

DOI: 10.1103/PhysRevB.103.224406

## I. INTRODUCTION

To compete with modern electronics, systems of spintronics—the spin analog of electronics—are becoming smaller. In turn, mesoscopic effects become more important. On the one hand, this complicates the description of spintronic effects. On the other hand, however, it opens up new ways to investigate and manipulate spintronic systems. Here, we demonstrate how the Coulomb blockade—a prominent effect of mesoscopic physics—can be used to measure magnetization dynamics via a system's current-voltage characteristics.

We consider a single tunnel junction between a normal metal and a metallic ferromagnet (see Fig. 1). A tunnel junction is a thin insulating layer which separates two metallic systems (leads) from each other. Classically, a tunnel junction forms a capacitor, as the insulating layer separates the two metallic systems by a small distance. Quantum mechanically—as the name "tunnel junction" suggests—electrons can tunnel through the insulating layer. The classical and quantum perspectives are related: when an electron tunnels through the junction, it changes the charge on the capacitor and, in turn, it changes the electrostatic Coulomb energy stored in the capacitor [1,2]. If an electron does not have enough energy to compensate the cost in Coulomb energy, then the tunneling is blocked; this is the Coulomb blockade [1,2].

The energy to overcome the Coulomb blockade can come from thermal fluctuations, from the voltage source, or—in the present case—from the magnetization dynamics. To focus on the role of the magnetization dynamics, we consider the limit of zero temperature. For simplicity, we assume that the magnetization precesses in a steady state and, we use the macrospin approximation; that is, we describe the magnetization as a single vector $\boldsymbol{M}$. A precessing macrospin (magnetization) acts as a time-dependent magnetic field for electrons and—as a special case of adiabatic pumping [3,4]—pumps spin-polarized electrons into adjacent leads [5–7]. For a tunnel junction, this means that a precessing macrospin can assist electrons in tunneling [8] (see also [9,10]).

In this paper, we study the competition between Coulomb blockade and macrospin-assisted tunneling. This places our work into the emerging field of mesoscopic spintronics. Other topics in this field include, for example, the study of

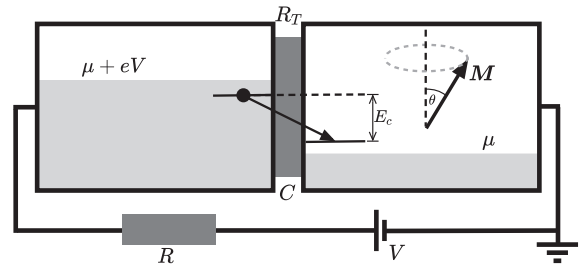


FIG. 1. We consider a single tunnel junction between a normal metal (left lead) and a metallic ferromagnet (right lead) with a magnetization in a steady-state precession. Separating two metallic systems, the tunnel junction forms a capacitor (capacitance $C$). For $R \gg R_K = h/e^2$, an electron, when tunneling, changes the charge on the capacitor by $e$ and, in turn, it loses the charging energy ($E_c = e^2/2C$) to its electrostatic environment [1,2]. For low voltage ($eV < E_c$) and low temperature ($k_bT \ll E_c$), this energy loss usually forbids charge transport (Coulomb blockade). However, we show that the precessing magnetization can break the Coulomb blockade by assisting electrons in tunneling.

 

noise in spintronics [8,11–17], the mesoscopic Stoner instability [18–21], and spintronics with quantum dots [22–27], which is closely related to our work. Here, we show that the macrospin-assisted tunneling can provide enough energy to overcome the Coulomb blockade. Therefore, the macrospin-assisted tunneling softens or even breaks the Coulomb blockade and, as a result, the system's current-voltage characteristics reveal the macrospin dynamics.

For slow precession, the macrospin-assisted tunneling softens the Coulomb blockade (see Fig. 2). For strong precession, the macrospin-assisted tunneling breaks the Coulomb blockade (see Fig. 3). In both cases, the macrospin dynamics governs the flow of the charge current. Read in reverse, the charge current can be used to measure the magnetization dynamics (see Figs. 2 and 3). To be more explicit, we choose the macrospin's precession axis as the $z$ direction. The precessing macrospin is then described by $\boldsymbol{M} = M(\sin\theta\cos\phi, \sin\theta\sin\phi, \cos\theta)$, where polar angle $\theta$ and precession frequency $\dot{\phi}$ are constant. Roughly speaking, the polar angle $\theta$ can be inferred from the tunnel junction's differential conductance, while the precession frequency $\dot{\phi}$ can be inferred from the combined information of conductance and differential conductance. Alternatively, one can infer $\theta$ and $\dot{\phi}$ from the position of kinks in the current-voltage characteristics (see Figs. 2 and 3).

We close the Introduction by relating our work to Ref. [28], where the effect of an electromagnetic environment was studied for a magnetic tunnel junction with one precessing magnetization. Using $P(E)$ theory, they derived a general expression for the charge current which should also cover our result [29]. However, their focus was on open circuits, where no charge current can flow and a voltage buildup is predicted instead. In open circuits—with always vanishing charge current—the Coulomb blockade and its breaking cannot be seen directly. In contrast to their work, we use a simple Fermi's golden rule approach, treat the electrical environment classically, and focus on closed circuits. While less general, our simple approach makes the physics particularly transparent. So we can easily see how macrospin-assisted tunneling breaks the Coulomb blockade. In retrospect, we can even identify the results of Ref. [28] as important indirect signs of the breaking of Coulomb blockade by macrospin-assisted tunneling.

## II. THE MODEL

The breaking of the Coulomb blockade by macrospin-assisted tunneling can be found within a simple model: the electrons are described quantum mechanically by single-particle Hamiltonians, whereas the Coulomb energy is taken into account on the classical level.

The magnetic right lead is described by $H_r = \sum_{\rho\sigma\sigma'} |\rho\sigma\rangle h_{r,\rho}^{\sigma\sigma'} \langle\rho\sigma'|$, where $\sigma$ and $\sigma'$ denote the spin in the $z$ direction (the magnetization's precession axis), $\rho$ denotes the right-lead states with corresponding energy $\epsilon_\rho$, and $h_{r,\rho} = \epsilon_\rho - \boldsymbol{M}\boldsymbol{\sigma}/2$, with the vector of Pauli matrices $\boldsymbol{\sigma}$ and, for simpler notation, the magnetization length $M$ includes all constants [30]. The left lead is described by $H_l = \sum_{\lambda\sigma} |\lambda\sigma\rangle\epsilon_\lambda\langle\lambda\sigma|$, where $\lambda$ denotes the left-lead states with the corresponding energy $\epsilon_\lambda$. We assume spin-conserved tunneling, described by $H_t = \sum_{\lambda\rho\sigma} |\rho\sigma\rangle t_0 \langle\lambda\sigma| + \text{H.c.}$, where $t_0$ are the tunneling amplitudes between states $\rho$ and $\lambda$; for simplicity, we disregard the state dependence of $t_0$.

In addition to the Hamiltonian, we need to specify the distribution functions. We assume the tunneling events are rare, such that local equilibrium is reestablished before each tunneling event. Then, the electrons are distributed according to the Fermi distribution $f(\epsilon) = 1/\{\exp[(\epsilon-\mu)/T]+1\}$, where we assume the chemical potential $\mu$ and the temperature $T$ are equal in both leads. We emphasize, however, that $\mu$ is only the *chemical* potential, not the *electrochemical* potential.

## III. THE COULOMB BLOCKADE REGIME

The (electrostatic) Coulomb energy is taken into account in addition to the single-particle contributions. In the circuit (Fig. 1), there are two different scales for the electrostatic energy: first, there is $eV$, which is the work done by the voltage source when one electron is pumped from one side to the other; second, there is $Q^2/(2C)$, which is the energy stored in the capacitor with capacitance $C$ and charge $Q$. Which of these energy scales is relevant for the tunneling of electrons? As discussed in Ref. [1], the answer strongly depends on the tunnel junction's environment. In particular, it depends on the environmental resistance $R$: for a small resistance $R \ll R_K$, the (ideal) voltage source fixes the charge on the capacitor to $Q = CV$, such that the energy stored in the capacitor remains fixed and, the tunneling is governed by the voltage source; for large resistance $R \gg R_K$, in contrast, the voltage source cannot immediately restore the charge on the capacitor, such that the capacitor's energy governs the tunneling. The natural scale separating these two cases is the resistance quantum (von Klitzing constant) $R_K = h/e^2$ [1]. In the following, we focus on $R \gg R_K$ and the limit of zero temperature $T = 0$, which puts the system into the Coulomb blockade regime.

An electron can tunnel only if it has enough energy available. When one electron tunnels, the charge on the capacitor $Q$ is changed by $-e$ for left-to-right tunneling and by $+e$ for right-to-left tunneling. So the change in electrostatic energy is $\Delta E_{el} = Q^2/2C - (Q \mp e)^2/2C$. Assuming tunneling events are rare, the capacitor is recharged to $Q = CV$ before each tunneling event [31]. In turn, we find $\Delta E_{el} = \pm eV - E_c$ with the charging energy $E_c = e^2/2C$. If the applied voltage is too small ($\Delta E_{el} < 0$), we enter the regime of Coulomb blockade, where electrons cannot tunnel unless the missing electrostatic energy is supplied in a different way [1,2]. At $T = 0$, the missing energy cannot come from thermal activation. However, the precessing macrospin can assist electrons in tunneling [8] and, thereby, it provides the missing energy.

## IV. MACROSPIN-ASSISTED TUNNELING

As a first step, we determine the tunneling rate between states in the left lead and states in the right lead. We assume the tunnel coupling is a weak perturbation, such that we can use Fermi's golden rule.

Before Fermi's golden rule can be applied, we have to change to the magnetization's rotating frame of reference, such that the leads' Hamiltonians become time independent. So following Ref. [8], we apply a transformation

$U(t) = \sum_{\rho\sigma} |\rho\sigma;\boldsymbol{M}(t)\rangle\langle\rho\sigma| + \sum_{\lambda\sigma} |\lambda\sigma\rangle\langle\lambda\sigma|$, where $|\rho\sigma;\boldsymbol{M}(t)\rangle$ is an instantaneous eigenstate of $\boldsymbol{M}(t)\hat{\boldsymbol{\sigma}}$; formally, $\boldsymbol{M}(t)\hat{\boldsymbol{\sigma}}|\rho\sigma;\boldsymbol{M}(t)\rangle = M\sigma\,|\rho\sigma;\boldsymbol{M}(t)\rangle$, with $M = |\boldsymbol{M}|$. This transformation does not affect the left lead's Hamiltonian $\tilde{H}_l := UH_lU^\dagger = H_l$. But it diagonalizes the right lead's Hamiltonian $\tilde{H}_r := UH_rU^\dagger = \sum_{\rho\sigma} |\rho\sigma\rangle\xi_{\rho\sigma}\langle\rho\sigma|$, where $\xi_{\rho\sigma} = \epsilon_\rho - M\sigma/2$. The magnetization's time dependence is transferred to the tunneling Hamiltonian $\tilde{H}_t := UH_tU^\dagger = \sum_{\rho\lambda\sigma\sigma'} |\rho\sigma\rangle[R^\dagger(t)]_{\sigma\sigma'}t_0\langle\lambda\sigma'| + \text{H.c.}$ That is, the tunneling amplitudes become time dependent and nontrivial in spin space,

$$t_0 \to R^\dagger(t)\,t_0. \tag{1}$$

The spin-space rotation $R(t)$ is defined by its elements $[R(t)]_{\sigma\sigma'} := \langle\rho\sigma;\boldsymbol{M}(t)|\rho\sigma'\rangle$. Note, however, that this definition is not unique, as a rotation around the magnetization direction (spin quantization axis) has no physical effect. This gives rise to a gauge freedom which can be used to simplify the calculation [15].

Due to its time dependence, the transformation not only rotates the Hamiltonian but it also generates a new term, $-iU\dot{U}^\dagger = -i\sum_{\rho\sigma\sigma'} |\rho\sigma\rangle[R^\dagger\dot{R}]_{\sigma\sigma'}\langle\rho\sigma'|$, in the rotating-frame Hamiltonian. The spin-off-diagonal part of $-iR^\dagger\dot{R}$ induces transitions, also known as Landau-Zener transitions, between spin-up and spin-down states. However, we assume a large magnetization length $M$, such that we can disregard these transitions [32]; this is also known as adiabatic approximation [15]. The remaining spin-diagonal part of $-iR^\dagger\dot{R}$ gives an additional time-evolution phase, also known as Berry phase, which is different for spin-up and spin-down states. However, we eliminate the spin-diagonal part of $-iR^\dagger\dot{R}$ by fixing the gauge analog to Ref. [15]; that is, we explicitly choose

$$R(t) = \begin{pmatrix} \cos\frac{\theta}{2}\, e^{-i\omega_- t} & -\sin\frac{\theta}{2}\, e^{-i\omega_+ t} \\ \sin\frac{\theta}{2}\, e^{i\omega_+ t} & \cos\frac{\theta}{2}\, e^{i\omega_- t} \end{pmatrix}, \tag{2}$$

with $\omega_\pm = \dot{\phi}(1 \pm \cos\theta)/2$, where $\omega_-$ is the rate at which the Berry phase is acquired. Even though this choice eliminates the spin-diagonal part of $-iR^\dagger\dot{R}$, it does not eliminate the Berry phase. Instead, the Berry phase is transferred to the tunneling elements, Eq. (1). To summarize, for the specific choice, Eq. (2), the newly generated term $-iR^\dagger\dot{R}$ can be disregarded in an adiabatic approximation.

Now, in the rotating frame, it is straightforward to apply Fermi's golden rule. Treating the tunneling Hamiltonian $\tilde{H}_t$ as perturbation, we obtain the golden-rule rate,

$$\Gamma_{\lambda\sigma'\rightleftarrows\rho\sigma} = \frac{2\pi}{\hbar}|t_0|^2\frac{1+\sigma\sigma'\cos\theta}{2} \times \delta(\xi_{\rho\sigma} - \epsilon_\lambda + \sigma'\hbar\omega_{\sigma\sigma'} - eV \pm E_c), \tag{3}$$

where $+E_c$ and $-E_c$ correspond to left-to-right tunneling $\lambda\sigma' \to \rho\sigma$ and right-to-left tunneling $\rho\sigma \to \lambda\sigma'$, respectively. The *macrospin orientation* governs the spin-projection factor $(1+\sigma\sigma'\cos\theta)/2$, which is $\cos^2\frac{\theta}{2}$ for equal spins $\sigma = \sigma'$ and $\sin^2\frac{\theta}{2}$ for opposite spins $\sigma \neq \sigma'$. The *macrospin dynamics* enters through the frequency $\omega_{\sigma\sigma'} = \dot{\phi}(1-\sigma\sigma'\cos\theta)/2$, which is $\omega_-$ for equal spins $\sigma = \sigma'$ and $\omega_+$ for opposite spins $\sigma \neq \sigma'$. In the rotating frame, the macrospin dynamics translates into the time dependence of the perturbation [tunneling Hamiltonian; see Eqs. (1) and (2)]. Consequently, the macrospin dynamics induces the energy shift $\sigma'\hbar\omega_{\sigma\sigma'}$ in the golden-rule rate. In other words, the precessing macrospin gives energy to—or takes energy from—the tunneling electrons; that is, it can assist electrons in tunneling [8].

Now, knowing the golden-rule rate, Eq. (3), we can determine the charge current.

## V. CHARGE CURRENT

The net charge current $I = I_{l\to r} - I_{r\to l}$ is the difference between the left-to-right current $I_{l\to r}$ and the right-to-left current $I_{r\to l}$.

First, we focus on the left-to-right current $I_{l\to r}$; that is, we consider only electrons that are tunneling from the left lead to the right lead. Formally, it is given by $I_{l\to r} = e\sum_{\rho\lambda\sigma\sigma'}\Gamma_{\lambda\sigma'\to\rho\sigma}f(\epsilon_\lambda)[1-f(\xi_{\rho\sigma})]$, where the golden-rule rate, Eq. (3), is summed over all states and—since electrons can tunnel only from filled states into empty states—it is weighted by the filling factor $f(\epsilon_\lambda)$ and the Pauli-blocking factor $[1-f(\xi_{\rho\sigma})]$. More explicitly,

$$I_{l\to r} = \frac{g_t}{2e}\sum_{\sigma\sigma'}\frac{1+\sigma\sigma'\cos\theta}{2} \times \int d\epsilon_l \int d\epsilon_r\, f(\epsilon_l - eV)[1-f(\epsilon_r)] \times \delta(\epsilon_r - \epsilon_l + E_c + \sigma'\hbar\omega_{\sigma\sigma'}), \tag{4}$$

where we shifted the integrals $\epsilon_l \to \epsilon_l - eV$ and $\epsilon_r \to \epsilon_r + M\sigma/2$. Furthermore, we assumed the densities of states $\rho_l$ and $\rho_r$ were constant on all scales smaller than $M$ and independent of the spin [33]. The tunneling conductance $g_t$ is defined by $g_t = 8\pi^2|t_0|^2\rho_l\rho_r\,e^2/h$. From Eq. (4), it becomes clear that $eV$ is just the electrical part of the electrochemical potential: $f(\epsilon_l - eV) = 1/\{\exp[(\epsilon_l - \mu_l)/T] + 1\}$, where $\mu_l = \mu + eV$ is the electrochemical potential of the left lead.

For infinite capacitance ($E_c = 0$) and without magnetization dynamics ($\omega_{\sigma\sigma'} = 0$), the $\delta$ function in Eq. (4) ensures the conservation of energy for the tunneling electrons. For finite capacitance, however, a tunneling electron loses the charging energy $E_c$ to the electrostatic environment (capacitor) [1,2]; see Fig. 1. The energy shift $\sigma'\hbar\omega_{\sigma\sigma'}$ accounts for the effect of the macrospin dynamics on the tunneling electron; namely, it describes the energy gain or loss due to the macrospin precession. Performing the integrals in Eq. (4), we obtain

$$I_{l\to r} = \frac{g_t}{2e}\Big[\cos^2\frac{\theta}{2}\,\Pi(eV - E_c - \hbar\omega_-) + \sin^2\frac{\theta}{2}\,\Pi(eV - E_c + \hbar\omega_+) + \sin^2\frac{\theta}{2}\,\Pi(eV - E_c - \hbar\omega_+) + \cos^2\frac{\theta}{2}\,\Pi(eV - E_c + \hbar\omega_-)\Big], \tag{5}$$

where $\Pi(x)$ is the ramp function; that is, $\Pi(x) = 0$ for $x \leqslant 0$, and $\Pi(x) = x$ for $x > 0$. The four terms in $I_{l\to r}$ arise from the different combinations of spins in left-to-right tunneling.

The right-to-left current $I_{r\to l}$ can be found analogously to the left-to-right current $I_{l\to r}$; only the roles of the leads are exchanged [34]. Combining both, we find that the charge current, $I = I_{l\to r} - I_{r\to l}$, is antisymmetric in the voltage; that is, $I(-V) = -I(V)$. This is a consequence of assuming the densities of states are spin independent.

To gain a better understanding of the charge current, let us consider a situation with static macrospin ($\dot{\phi} = 0$) at first. In the limit of infinite capacitance ($E_c = 0$), the tunnel junction behaves as a resistor; that is, the current-voltage relation is described by Ohm's law $I = g_t V$. For finite capacitance ($E_c > 0$), in contrast, the tunneling electrons lose the energy $E_c$ to the electrostatic environment. This loss effectively reduces the voltage by $E_c/e$. Consequently, we obtain $I = g_t[(V - E_c/e)\,\Theta(V - E_c/e) - (-V - E_c/e)\,\Theta(-V - E_c/e)]$, which is the standard Coulomb blockade result [1,2]: if the voltage is too low ($|eV| < E_c$), the charge transport is blocked ($I = 0$). However, when the macrospin precesses ($\dot{\phi} \neq 0$), it can assist electrons in tunneling; therefore, it softens the Coulomb blockade, or if the precession is strong enough, it can even break the Coulomb blockade.

## VI. BREAKING OF THE COULOMB BLOCKADE

When the macrospin precesses slowly ($\hbar|\dot{\phi}| < E_c$), the Coulomb blockade is softened: electrons can tunnel through the junction, even if the applied voltage is smaller than, but close enough to, the charging energy (see Fig. 2). The missing energy is provided by the precessing macrospin. So the macrospin dynamics governs the softening of the Coulomb blockade. In turn, a measurement of the charge current can reveal the macrospin dynamics. For example in the voltage regime $E_c - \hbar|\omega_+| < eV < E_c - \hbar|\omega_-|$ (compare Fig. 2), the current is given by $I = g_t \sin^2(\theta/2)[eV - E_c + \hbar|\dot{\phi}|\cos^2(\theta/2)]/2e$. Thus, a measurement of the differential conductance $\frac{dI}{dV} = \sin^2(\theta/2)g_t/2$ gives information about the polar angle $\theta$. Then, knowing $\sin^2(\theta/2)$, the precession frequency $|\dot{\phi}|$ can be inferred from the current $I$ itself. A shortcoming of this method is that one has to know in which regime the voltage is. A simpler way would be to measure the current-voltage characteristics (Fig. 2) and get information about the magnetization dynamics from the position of the kinks at $E_c \pm \hbar|\omega_+|$ and $E_c \pm \hbar|\omega_-|$—or, analogously, from the position of jumps in the differential conductance.

While only softened for slow precession, the Coulomb blockade is completely broken for strong macrospin precession ($\hbar|\omega_+| > E_c$ and/or $\hbar|\omega_-| > E_c$). In this case, the precessing macrospin gives enough energy to the tunneling electrons, such that tunneling is possible even if there is no other source of energy. In turn, even at low voltages, we find a linear relation between current and voltage (see Fig. 3). So the macrospin dynamics governs the breaking of the Coulomb blockade. Again, a measurement of the charge current can reveal the macrospin dynamics. However, in contrast to the softening of the Coulomb blockade, the (differential) conductance can reveal the polar angle $\theta$ even at zero voltage. For example, in the low-voltage regime ($E_c - \hbar|\omega_+| < eV < -E_c + \hbar|\omega_+|$), as shown in Fig. 3, the current is given by $I = g_t V \sin^2(\theta/2)$, which gives information about the polar angle $\theta$ but not about the precession frequency $|\dot{\phi}|$ [35]. To determine the precession frequency, one has to go to higher voltages again.

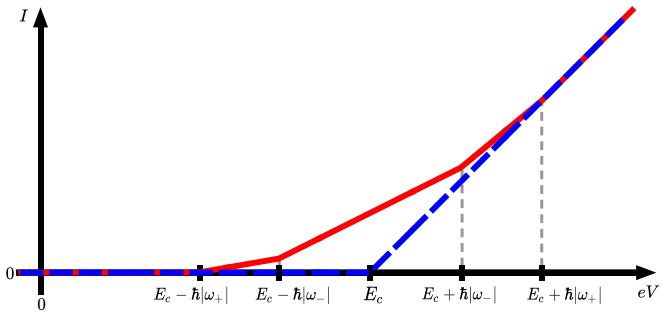


FIG. 2. The softening of the Coulomb blockade for slow precession ($\hbar|\dot{\phi}| < E_c$) with $0 < \theta < \pi/2$. While charge transport is still blocked for low voltages, due to macrospin-assisted tunneling a current flows already for $eV > E_c - \hbar|\omega_+|$. The details of the current flow depend on the macrospin dynamics. Thus, the macrospin dynamics can be measured (indirectly) by the charge current. The standard Coulomb blockade is included as a reference (blue dashed line).

## VII. DISCUSSION

We have found that macrospin-assisted tunneling can break the Coulomb blockade. More explicitly, we considered a tunnel junction between a normal metal and a metallic ferromagnet where the macrospin (magnetization) is in a steady-state precession. The precessing macrospin creates a time-dependent field for electrons, which can assist them in tunneling [8]. As we have shown, this macrospin-assisted tunneling shrinks the regime of the Coulomb blockade (see Fig. 2). When the macrospin precession is strong enough, the regime of the Coulomb blockade vanishes completely (see Fig. 3). In other words, the macrospin-assisted tunneling can soften or even break the Coulomb blockade. The details of the softening or breaking of Coulomb blockade depend on the macrospin dynamics. Thus, a measurement of the charge current can reveal the macrospin dynamics.

To get a better understanding of the scales involved, let us consider a specific system. For example, in Ref. [36], the authors reported on a magnetic tunnel junction with an elliptical shape (minor axis of 40 nm, major axis of 80 nm) and a MgO tunnel barrier with a thickness of 0.9 nm. This geometry (and material) leads to a capacitance of $C \approx 0.25$ fF for the tunnel junction [37]. In turn, we find a charging energy of $E_c \approx 0.32$ meV which corresponds to a temperature of $T_c = E_c/k_B \approx 3.7$ K and a frequency of $f_c = E_c/h \approx 78$ GHz. To enter the regime of Coulomb blockade, the temperature must be well below $T_c$. Then, the precessing macrospin could break the Coulomb blockade if it precesses at frequencies above $f_c$. While the precession frequency reported in Ref. [36] is only of the order of 10 GHz, it is still close enough to the critical frequency $f_c$, such that one can expect a clear softening of the Coulomb blockade, analogous to Fig. 2. For a tunnel junction of larger dimensions and with a thinner barrier, the critical frequency $f_c$ can fall below 10 GHz such that one might also

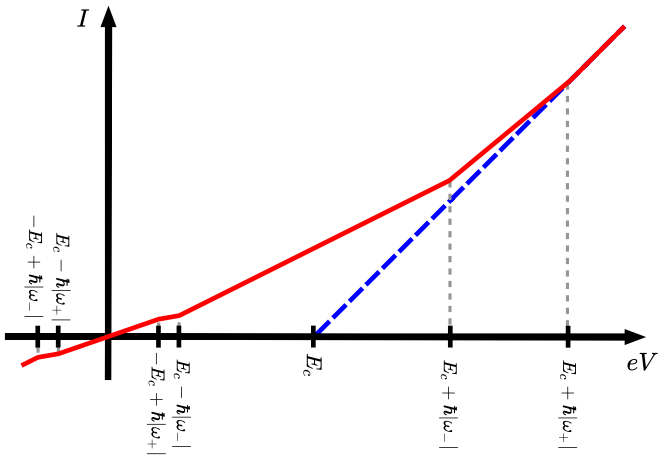


FIG. 3. The breaking of the Coulomb blockade for strong macrospin precession ($\hbar|\omega_+| > E_c$) with $0 < \theta < \pi/2$. The standard Coulomb blockade is included as a reference (blue dashed line). Because of the macrospin-assisted tunneling, the Coulomb blockade disappears; that is, a charge current flows at arbitrary low (but nonzero) voltages. Yet the details depend on the macrospin dynamics. In turn, measuring the charge current can reveal the macrospin dynamics.

observe the breaking of the Coulomb blockade, analogous to Fig. 3.

Also beyond the specific setup considered here, the breaking of the Coulomb blockade by macrospin-assisted tunneling might be interesting, in particular, for scanning tunneling microscope (STM) setups [28]. In STM setups, the capacitance is harder to estimate (see Ref. [38], for example). However, in Ref. [39], where the authors also used the Coulomb blockade to investigate a system in a scanning tunneling spectroscopy setup, they found a junction capacitance of $C = 21.7\,\mathrm{fF}$. This capacitance corresponds to a charging energy of $E_c \approx 3.7\,\mu\mathrm{eV}$, a temperature of $T_c = E_c/k_B \approx 42\,\mathrm{mK}$, and a frequency of $f_c = E_c/h \approx 0.9\,\mathrm{GHz}$. So in this case, a macrospin precession frequency of roughly 10 GHz would be well above $f_c$, such that the macrospin-assisted tunneling can easily break the Coulomb blockade. This effect might be particularly interesting for resonant-state-STM setups [40,41], where the charging energy $E_c$ can be tuned, because of the large variability in the distance between the STM tip and probe material.

While we focused on a passive use (indirect measurement of magnetization dynamics), we can also think of more active uses of the interplay between the Coulomb blockade and macrospin-assisted tunneling. It could be used to control a spin current electrically [42]. Or when the magnet's density of states is spin dependent, it could be used to pump a charge current [43]. Because it can be used to control spin and charge currents, it might also open up new ways to control the magnetization dynamics. From a more general perspective, the interplay between Coulomb blockade and macrospin-assisted tunneling provides a new platform for the interplay between electronics and spintronics. From this perspective, magnon-assisted tunneling (as considered in [9,10,44–46]) is a natural candidate for the generalization of our results.

## ACKNOWLEDGMENTS

We thank I. S. Burmistrov, P. Simon, M. Trif, and W. Wulfhekel for a fruitful discussion. This work is part of the research program Fluid Spintronics under Project No. 182.069, which is (partly) financed by the Dutch Research Council (NWO).

[1] G.-L. Ingold and Y. V. Nazarov, Charge tunneling rates in ultrasmall junctions, in *Single Charge Tunneling* (Springer, Boston, MA, 1992), pp. 21–107.

[2] Y. V. Nazarov and Y. M. Blanter, *Quantum Transport: Introduction to Nanoscience* (Cambridge University Press, Cambridge, 2009).

[3] P. W. Brouwer, Scattering approach to parametric pumping, Phys. Rev. B **58**, R10135 (1998).

[4] P. W. Brouwer, Rectification of displacement currents in an adiabatic electron pump, Phys. Rev. B **63**, 121303(R) (2001).

[5] Y. Tserkovnyak, A. Brataas, and G. E. W. Bauer, Enhanced Gilbert Damping in Thin Ferromagnetic Films, Phys. Rev. Lett. **88**, 117601 (2002).

[6] A. Brataas, Y. Tserkovnyak, G. E. W. Bauer, and B. I. Halperin, Spin battery operated by ferromagnetic resonance, Phys. Rev. B **66**, 060404(R) (2002).

[7] Y. Tserkovnyak, A. Brataas, G. E. W. Bauer, and B. I. Halperin, Nonlocal magnetization dynamics in ferromagnetic heterostructures, Rev. Mod. Phys. **77**, 1375 (2005).

[8] T. Ludwig, I. S. Burmistrov, Y. Gefen, and A. Shnirman, Current noise geometrically generated by a driven magnet, Phys. Rev. Res. **2**, 023221 (2020).

[9] S. Zhang, P. M. Levy, A. C. Marley, and S. S. P. Parkin, Quenching of Magnetoresistance by Hot Electrons in Magnetic Tunnel Junctions, Phys. Rev. Lett. **79**, 3744 (1997).

[10] S. A. Bender, R. A. Duine, and Y. Tserkovnyak, Quantum-kinetic theory of spin-transfer torque and magnon-assisted transport in nanoscale magnetic junctions, Phys. Rev. B **99**, 024434 (2019).

[11] F. Aliev and J. P. Cascales, *Noise in Spintronics: From Understanding to Manipulation* (CRC Press, Boca Raton, FL, 2018).

[12] J. P. Cascales, D. Herranz, F. G. Aliev, T. Szczepański, V. K. Dugaev, J. Barnaś, A. Duluard, M. Hehn, and C. Tiusan, Controlling Shot Noise in Double-Barrier Magnetic Tunnel Junctions, Phys. Rev. Lett. **109**, 066601 (2012).

[13] A. Kamra and W. Belzig, Spin Pumping and Shot Noise in Ferrimagnets: Bridging Ferro- and Antiferromagnets, Phys. Rev. Lett. **119**, 197201 (2017).

[14] A. Kamra and W. Belzig, Super-Poissonian Shot Noise of Squeezed-Magnon Mediated Spin Transport, Phys. Rev. Lett. **116**, 146601 (2016).

[15] A. Shnirman, Y. Gefen, A. Saha, I. S. Burmistrov, M. N. Kiselev, and A. Altland, Geometric Quantum Noise of Spin, Phys. Rev. Lett. **114**, 176806 (2015).

[16] P. Virtanen and T. T. Heikkilä, Spin Pumping and Torque Statistics in the Quantum Noise Limit, Phys. Rev. Lett. **118**, 237701 (2017).

[17] A. Brataas, Current fluctuations driven by ferromagnetic and antiferromagnetic resonance, Phys. Rev. B **102**, 054440 (2020).

[18] I. L. Kurland, I. L. Aleiner, and B. L. Altshuler, Mesoscopic magnetization fluctuations for metallic grains close to the Stoner instability, Phys. Rev. B **62**, 14886 (2000).

[19] B. Sothmann, J. König, and Y. Gefen, Mesoscopic Stoner Instability in Metallic Nanoparticles Revealed by Shot Noise, Phys. Rev. Lett. **108**, 166603 (2012).

[20] A. Saha, Y. Gefen, I. Burmistrov, A. Shnirman, and A. Altland, A quantum dot close to Stoner instability: The role of the Berry phase, Ann. Phys. (NY) **327**, 2543 (2012).

[21] I. S. Burmistrov, Y. Gefen, D. S. Shapiro, and A. Shnirman, Mesoscopic Stoner Instability in Open Quantum Dots: Suppression of Coleman-Weinberg Mechanism by Electron Tunneling, Phys. Rev. Lett. **124**, 196801 (2020).

[22] J. König and J. Martinek, Interaction-Driven Spin Precession in Quantum-Dot Spin Valves, Phys. Rev. Lett. **90**, 166602 (2003).

[23] M. Braun, J. König, and J. Martinek, Theory of transport through quantum-dot spin valves in the weak-coupling regime, Phys. Rev. B **70**, 195345 (2004).

[24] S. A. Bender, Y. Tserkovnyak, and A. Brataas, Microwave response of a magnetic single-electron transistor, Phys. Rev. B **82**, 180403(R) (2010).

[25] N. Winkler, M. Governale, and J. König, Theory of spin pumping through an interacting quantum dot tunnel coupled to a ferromagnet with time-dependent magnetization, Phys. Rev. B **87**, 155428 (2013).

[26] M. Hell, B. Sothmann, M. Leijnse, M. R. Wegewijs, and J. König, Spin resonance without spin splitting, Phys. Rev. B **91**, 195404 (2015).

[27] N. M. Gergs, S. A. Bender, R. A. Duine, and D. Schuricht, Spin Switching via Quantum Dot Spin Valves, Phys. Rev. Lett. **120**, 017701 (2018).

[28] M. Trif and P. Simon, Giant magnetoelectric effect in magnetic tunnel junctions coupled to an electromagnetic environment, Phys. Rev. B **90**, 174431 (2014).

[29] Unfortunately, there is a typographical error in their Eq. (8): what they call $V_s$ and $T_s(\theta)$ (where $s = \pm$) should always come with opposite signs; that is, $V_+$ should come with $T_-(\theta)$, and $V_-$ should come with $T_+(\theta)$. Once that is corrected, their Eq. (8) includes our Eq. (5) as a limiting case.

[30] In detail, $M = \hbar\mu_0\mu_B g\bar{M}$, where $\bar{M}$ is the real magnetization and we assumed the external magnetic field is negligible, $\hbar$ is the reduced Planck constant, $\mu_0$ is the vacuum permeability, $\mu_B = e\hbar/2m_e$ is the Bohr magneton, and $g$ is the Landé $g$ factor.

[31] This assumption restricts our model to low currents. Electrons with charge $e$ are tunneling one by one, and the timescale for recharging the capacitor is $\tau_{RC} = RC$, which leads to an upper bound of charge current $I_{\max} = e/\tau_{RC} = e/RC = 2E_c/eR$; that is, for larger currents our model does not apply. To get a rough idea for the order of magnitude of $I_{\max}$, let us assume environmental resistance $R = 10\,R_K$ and charging energy $E_c = 0.32\,\text{meV}$ (compare Sec. VII). In this case, our model would be valid up to currents of approximately $I_{\max} \approx 2.5\,\text{nA}$.

[32] Via $\dot{R}$, the term $-iR^\dagger\dot{R}$ is related to the dynamics of the magnetization. So it becomes smaller for slower magnetization dynamics. Explicitly, this can be seen from the spin-off-diagonal elements $-i[R^\dagger\dot{R}]_{\sigma\bar{\sigma}} = \frac{\dot{\phi}\sin\theta}{2}e^{-i\sigma\phi\cos\theta\,t}$, where $\bar{\sigma}$ denotes the spin opposite to $\sigma$. To disregard these spin-off-diagonal terms, they must be small compared to the spin-diagonal elements. In more physical terms, the magnetization must be slow compared to its length.

[33] Formally, the spin independence means $\rho_r(\epsilon - M/2) = \rho_r(\epsilon + M/2) = \rho_r$ .

[34] Formally, we have $I_{r\to l} = e\sum_{\rho\lambda\sigma\sigma'}\Gamma_{\rho\sigma\to\lambda\sigma'}f(\xi_{\rho\sigma})[1 - f(\epsilon_\lambda)]$. Explicitly, we obtain $I_{r\to l} = \frac{g_t}{2e}[\cos^2\frac{\theta}{2}\Pi(-eV - E_c + \hbar\omega_-) + \sin^2\frac{\theta}{2}\Pi(-eV - E_c - \hbar\omega_+) + \sin^2\frac{\theta}{2}\Pi(-eV - E_c + \hbar\omega_+) + \cos^2\frac{\theta}{2}\Pi(-eV - E_c - \hbar\omega_-)]$.

[35] Note, however, that this works only if either $|\hbar\omega_+| > E_c$ and $|\hbar\omega_-| < E_c$ or $|\hbar\omega_+| < E_c$ and $|\hbar\omega_-| > E_c$. If $|\hbar\omega_+| > E_c$ and $|\hbar\omega_-| > E_c$, then we would simply find Ohm's law, $I = g_t V$, at low voltages.

[36] J. P. Cascales, D. Herranz, U. Ebels, J. A. Katine, and F. G. Aliev, Detection of spin torque magnetization dynamics through low frequency noise, Appl. Phys. Lett. **107**, 052401 (2015).

[37] To estimate the capacitance, we used the formula for parallel plates $C = \epsilon_0\epsilon_r A/d$, with the dielectric constant $\epsilon_0 \approx 9 \times 10^{-12}\,\frac{\text{F}}{\text{m}}$, the relative permittivity for MgO (which is $\epsilon_r \approx 10$), the ellipsis area $A = \frac{\pi}{4}40 \times 80\,\text{nm}^2$, and the barrier thickness $d = 0.9\,\text{nm}$.

[38] J. De Voogd, M. Van Spronsen, F. Kalff, B. Bryant, O. Ostojić, A. Den Haan, I. Groot, T. Oosterkamp, A. Otte, and M. Rost, Fast and reliable pre-approach for scanning probe microscopes based on tip-sample capacitance, Ultramicroscopy **181**, 61 (2017).

[39] J. Senkpiel, J. C. Klöckner, M. Etzkorn, S. Dambach, B. Kubala, W. Belzig, A. L. Yeyati, J. C. Cuevas, F. Pauly, J. Ankerhold, C. R. Ast, and K. Kern, Dynamical Coulomb Blockade as a Local Probe for Quantum Transport, Phys. Rev. Lett. **124**, 156803 (2020).

[40] A. Schlenhoff, S. Kovařík, S. Krause, and R. Wiesendanger, Vacuum Resonance States as Atomic-Scale Probes of Noncollinear Surface Magnetism, Phys. Rev. Lett. **123**, 087202 (2019).

[41] A. Schlenhoff, S. Kovarik, S. Krause, and R. Wiesendanger, Real-space imaging of atomic-scale spin textures at nanometer distances, Appl. Phys. Lett. **116**, 122406 (2020).

[42] For example, for the softening of the Coulomb blockade, Fig. 2, we have a purely spin polarized current in the regime $E_c - |\hbar\omega_+| < eV < E_c - |\hbar\omega_-|$. In this regime, electrons tunnel only from spin-up states to spin-up states. And the number of tunneling electrons (the current) can be controlled by the applied voltage.

[43] The charge pumping is similar to that in Ref. [47], but interestingly, it works for a tunnel junction between a magnet and a normal metal, that is, without a second magnet.

[44] X.-F. Han, A. C. C. Yu, M. Oogane, J. Murai, T. Daibou, and T. Miyazaki, Analyses of intrinsic magnetoelectric properties in spin-valve-type tunnel junctions with high magnetoresistance and low resistance, Phys. Rev. B **63**, 224404 (2001).

[45] C. Lü, M. Wu, and X. Han, Magnon- and phonon-assisted tunneling in a high-magnetoresistance tunnel junction using $Co_{75}Fe_{25}$ ferromagnetic electrodes, Phys. Lett. A **319**, 205 (2003).

[46] T. Balashov, A. F. Takács, M. Däne, A. Ernst, P. Bruno, and W. Wulfhekel, Inelastic electron-magnon interaction and spin transfer torque, Phys. Rev. B **78**, 174404 (2008).

[47] Y. Tserkovnyak, T. Moriyama, and J. Q. Xiao, Tunnel-barrier-enhanced dc voltage signals induced by magnetization dynamics in magnetic tunnel junctions, Phys. Rev. B **78**, 020401(R) (2008).